Yoke-free magnetic system for low field studies in magnetically affected reaction yield spectroscopy

Evgeny V. Kalneus,[a] Dmitri V. Stass, and Yuri A. Grishin
Institute of Chemical Kinetics and Combustion SB RAS, and Novosibirsk State University, 630090 Novosibirsk, Russia

(Received 27 January 2005; accepted 14 June 2005; published online 28 July 2005)

The article reports the development of a specialized magnetic system for application in low field studies of chemical reactions involving paramagnetic intermediates. We have designed and built a yoke-free magnetic system optimized for creating rather low static homogeneous magnetic fields that can be cleanly swept through zero value. The actually built system creates magnetic field in the range from "−500" to "+500" G in a cylindrical working region with a length of 8 cm and a diameter of 1 cm with a relative field homogeneity of about 10^{-4} without using ferromagnetic elements or employing a field-sensing feedback loop. At a distance of greater than or equal to 15 cm from the center of the system along the sweeping axis, the magnetic field does not exceed 100 G due to active shielding, which allows putting magnetic field-sensitive elements of the installation that close to the sample. We have tried to provide a detailed account of the design choices we faced and the compromises we had reached for each key aspect of the system, being rather specific about the reasoning behind each decision. The system actually built was thoroughly tested to verify the assumptions made at the design and the calculation stages and to check their practical realizability. The system will serve as the basis of a magnetically affected reaction yield spectrometer that is currently being developed in our laboratory, but hopefully can also be used in a wider array of applications centered around studies in low magnetic fields. © *2005 American Institute of Physics.* [DOI: 10.1063/1.2001646]

I. INTRODUCTION

The discovery of spin polarization effects and the effects of magnetic fields on the course of chemical reactions in solutions in 1970s established a methodology of experimental research in chemical physics—the methodology of "spin chemistry."[1–3] The techniques of spin chemistry cover a wide class of processes in chemistry and biology which involve short-lived paramagnetic species: biradicals, metastable triplet excited states of molecules, pairs of radicals or radical ions, etc. as one of their critical stages. All these methods rely on application of external magnetic fields to induce changes in the collective spin state of the unpaired electrons in the paramagnetic intermediates in such a way that will eventually lead to some observable changes in an experimentally monitored value. In a typical experiment radical pairs are created with an x-ray pulse, laser flash, or stationary photo or x irradiation. The yield of reaction of recombination of two radicals, the intensity of recombination fluorescence, or the non-Boltzmannian distribution of nuclear spin orientations in the stable diamagnetic products of recombination (nuclear polarization) is observed as a function of applied static or oscillating magnetic fields.

Spin chemistry counterparts have been created for major conventional magnetoresonance techniques, time resolved and continuous wave (CW) electron spin resonance (ESR). If the peculiarities of the recombination kinetics and the pairwise evolution of the two spins in the pair are taken into account, the techniques can in principle provide the same spectroscopic information as their more conventional ancestors. Their most important advantage, however, is an exceptionally high sensitivity due to indirectness of detecting microwave (MW) absorption. In polarization techniques the tremendous boost in sensitivity is provided by the non-Boltzmannian population of the spin levels. In the techniques relying on product analysis the high sensitivity is attained by accumulation of the product over some time interval. In fluorescence methods using optical detection it is the "heaviness" of optical quanta as compared to MW quanta that allows their individual detection and provides a sensitivity of units of radical pairs in the sample, as compared to typical sensitivities of 10^{11}–10^{13} spins for an *X*-band CW ESR spectrometer. Stationary concentrations of about 10^3 pairs in the sample are already sufficient for photocurrent mode of detection. Then conventional field modulation with lock-in detection can be used to improve sensitivity.

Spin chemical magnetoresonance techniques alleviate the problem of sensitivity in terms of macroscopic stationary concentration of the observed species, and come to the principal limitation of the necessity to flip the spin of unpaired electron with the available MW field B_1 within the lifetime of the paramagnetic species.[4] Practically attainable B_1 values of about 1 G in the resonator of a typical *X*-band CW ESR spectrometer impose the lower limit of about 100 ns on the lifetime of, say, a radical pair. To probe into still shorter

[a]Author to whom correspondence should be addressed; electronic mail: kalneus@ns.kinetics.nsc.ru

times, either substantially higher MW powers are needed, or a different detection principle should be sought. And here the region of low magnetic field, usually avoided by magnetoresonance techniques, proves to be valuable. In the vicinity of zero magnetic field, up to a field comparable to internal magnetic interactions of unpaired electron spin with magnetic nuclei (10–100 G), completely different principles of observation and investigation of radical pairs can be used. These rely on internal properties of the coherent spin system and are similar to nonlinear optical phenomena, as opposed to linear response to weak external perturbation traditionally employed in ESR and NMR. Since spin evolution leading to the observed signal is here driven by internal magnetic interactions rather than external MW pumping, a system with substantial hyperfine couplings of about 100 G can bring about a 100-fold gain in short-time sensitivity at the cost of certain loss of spectral resolution of the traditional linear response techniques.

The method of magnetically affected reaction yield (MARY), or level crossing, spectroscopy as developed in the authors' lab takes advantage of narrow resonance-like lines on the dependence of the intensity of recombination fluorescence from the *X*-irradiated sample on external static magnetic field. The lines arise at zero and in weak (10–100 G) magnetic fields due to coherent evolution of the spin systems of radical ion pairs that are formed upon ionization of molecules in the sample. These are similar in nature to Hanle signals in the magnetic field depolarization of resonance fluorescence, which are used in high sensitivity weak magnetic field meters based on optically polarized alkali metal atoms.[5] Since the signals are rather weak, field modulation with lock-in detection and symmetric passage through zero field are normally used. The scheme of the currently used spectrometer built on the basis of a commercial Bruker ER200D CW ESR spectrometer is shown in Fig. 1. The details of the technique and the general look of the obtained MARY spectra can be found elsewhere.[6] The issues important for this work are that a liquid sample with linear dimensions of about 1 cm is to be placed in external static magnetic field that will be cleanly swept from about −100 to +100 G through zero. There should be an x-ray tube (XRT) for sample irradiation and a photomultiplier tube (PMT) for light detection as close to the sample as practical, both being rather sensitive to magnetic fields. In the following sections we shall provide an account of our design, build, and test procedures which have led to creation of a high-performance magnetic field system specifically tailored for the region of weak magnetic fields.

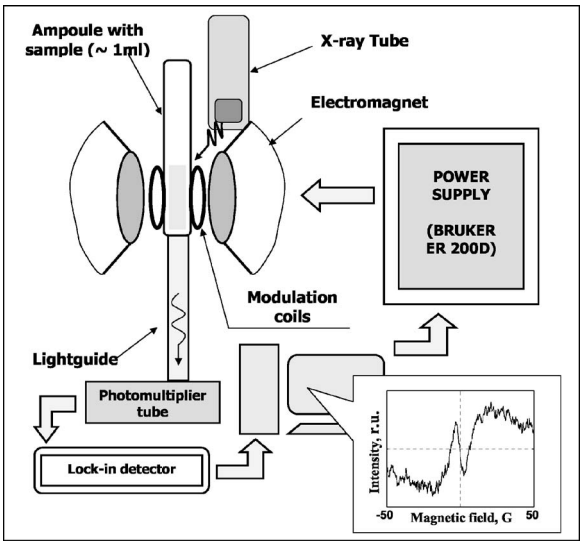

FIG. 1. Block scheme of MARY spectrometer. About 1 ml of liquid degassed sample in quartz ampoule is placed in the magnet of a commercial Bruker ER200D cw ESR spectrometer equipped with an x-ray tube (BSV-27 Mo, 40 kV × 40 mA) for sample irradiation and a PMT (FEU 130) for light detection. Magnetic field is modulated at 12.5 kHz using the modulation channel of the Bruker spectrometer. Furthermore, to shift the field to "negative" values for sweeping through zero, additional coils with dedicated power supply (not shown) are mounted on the poles of the magnet to create a constant static field of 50 G in the opposite direction, while all sweeping is performed by the Bruker console. The signal from the PMT is fed to Stanford Research System SR810 lock-in amplifier and then to computer for statistic averaging and processing. No microwave power is ever applied to the sample.

II. DESIGN CONSIDERATIONS

A. Experimental requirements and practical limitations

The overall requirements of the magnetic system have been formulated based on experimental experience with MARY spectroscopy. First we set the needed field sweep range. The primary MARY line is always observed at zero magnetic field (as are Hanle signals), however, occasionally lines in the field on the order of hyperfine couplings in the partners of the pair arise and bear important information.[7] To cover the entire important field range for the majority of organic radical ions with symmetric passage through zero, the region of field sweeping was chosen to be from −500 to +500 G.

The most important zero field line is also the narrowest line of the MARY spectrum. The lines in nonzero field, if present, are several times broader, with their width increasing as the line moves away from zero, and with still broader background of the spectrum—the regular magnetic field effect curve.[8] From the practical viewpoint it means that the highest absolute field homogeneity is required in the vicinity of zero field—as the field is increased, the requirements become more relaxed. We mention it specifically here because it is in contrast to normal ESR/NMR practice, where high absolute field homogeneities are required in rather strong fields, leading to very stringent demands on relative field homogeneity. The situation is different in MARY, and we shall take advantage of this. The narrowest zero field line observed to date had width of about 1 G, with much narrower lines theoretically possible,[9] so we set as a goal the requirement to cleanly record lines at least as narrow as 0.1 G in the vicinity of zero magnetic field. The practically attainable field homogeneity will be discussed later after the system is conceived.

An XRT tube is a "difficult" irradiation source to incorporate in a magnetic system. Due to short lifetimes, to tens of nanoseconds, of the generated radical ion pairs, as high a fluence of x-ray quanta as possible is desired to increase the rate of pair generation, and thus their stationary concentra-

tion in the sample. Currently we are operating a BSV-27Mo XRT at 40 kV×40 mA, which is close to the rated limit of the tube. This means that as much of the generated x-ray flux should be used as possible. On the other hand, an XRT irradiates in rather large solid angle, and the radiation is virtually impossible to focus or otherwise condition. This leads to x-ray fluence for a given sample size being inversely proportional to square of the sample-to-XRT distance. In fact, this is the reason for such a large linear sample size (1 cm). The closer the sample is to the XRT, the better. Currently the tube is at a distance of about 15 cm from the sample, which allows working in the photocurrent mode of light detection with a PMT at nearly the rated XRT power. Thus, the XRT should be placed no farther than 20 cm from the sample in the magnetic system.

On the other hand, the XRT is rather sensitive to magnetic fields. A simple estimate shows that for an accelerating voltage of 40 kV across a 1 cm gap, as in the currently used XRT, the electrons are deflected by as much as 6.5 mm in a magnetic field of 500 G, which is comparable to the linear dimensions of the water-cooled emitting target in the XRT. Operation of the XRT in high magnetic fields leads to very fast degradation of the tube and must be definitely avoided. In a field of 100 G the estimated deflection does not exceed 1 mm. Thus the maximum allowable field at the XRT location was defined as 100 G. The detecting PMT is also sensitive to magnetic field, but since the light can be transferred with good efficiency with a lightguide, this is not a serious problem.

Typical linear size of the sample in MARY spectroscopy is about 1 cm. If a field probe is required, it will be placed next to the sample. Furthermore, a temperature regulation arrangement for the sample is highly desired, which would move the probe still farther away from the sample. Finally, the probe must be protected from incident and stray *X* irradiation, so that some sort of absorber is required that would increase the sample-probe separation even more. If in these conditions the probe is still required to measure magnetic field at the sample location, the region of field homogeneity should be expanded to at least several cm from the sample location. It was set to a cylinder 1 cm in diameter extending ±4 cm from the sample. The XRT will be placed at the axis of the cylinder, so the field must drop rather steeply outside the region of homogeneity. Finally, there must be an opening of at least 5 cm to access the sample compartment.

B. Yoke versus yoke-free design

There are two common approaches to creation of static magnetic fields with the desired characteristics, a solenoid-type system of coils with a ferromagnetic (steel) core as used in conventional ESR spectrometers, and a yoke-free system of coils along the lines of Helmholz coils. The most important advantages of the core-type design are good confinement of the field, rather high current-to-field conversion ratio, and very good attainable field homogeneity with properly made pole pieces. This is the type of magnet that is currently in use in our lab. However, the most serious obstacle in the context of this project is the necessity to scan through the zero of the field with maximum possible linearity, since the most critical field interval for the planned studies is several Gauss around zero. Because of the core the produced field here will not be proportional to the current injected in the coils, which would require arranging a feedback loop with a field sensor. However, it is difficult to find a sensor that will operate from practically zero field up to hundreds of Gauss with reasonably short time constant for stable feedback operation during field sweeping in real time. The most common sensor types, fluxgates and Hall probes, are excellent for portions of this field range, but cannot cover it all. We also note that the sensor is not allowed to alter the field at the sample location, which rules out fluxgates or other sensors with compensation coils or flux concentrators.

This serious problem is inherently eliminated in a yoke-free design of a magnetic system. Here magnetic field is created by an arrangement of currents (coils) suspended in open space, and the field from each coil is a linear function of its current. Furthermore, the fields from different current elements simply add up vectorially in space, so the separate components of the field can be tailored individually and then superimposed as desired. Now the currents can be controlled rather than the fields, which is technically much simpler. A field probe is still desired, but will function simply as a monitor and thus can be rather slow. The price for these advantages is much lower efficiency of current to field conversion, the difficulty of field confinement, and the sensitivity to any ferromagnetic objects that might be present near the system, as well as poorer attainable field homogeneity as compared to core-type magnets. However, the positive aspects of the yoke-free design outweighed its shortcomings here, and it was adopted as the basis for the magnetic system. The components of the system will now be developed one at a time and then put together to create the target field.

C. System layout

The magnetic system is required to sweep the field in one direction, further referred to as the *Z* axis, through zero. Thus, we separate it into the sweeping *Z* system and the compensating *XY* system, which cancels the residual transversal components of the total field. The *Z* axis is the axis of the magnetic system, and the sweeping system is a symmetric arrangement of coaxial coils along the *Z* axis, with XRT and PMT placed on the axis at the two opposite ends of the system. The working region of the system is defined as a cylinder 8 cm long by 1 cm in diameter.

The sample compartment is a thick-walled metal "barrel," providing the mechanical skeleton for the rather heavy coils and ensuring their coaxiality, and attenuating low-frequency pickup at the mains frequency and its harmonics. Skin layer thickness for normal metals is about 1 cm at 50 Hz and decreases as the inverse square root of frequency. Although copper is a somewhat better conductor than aluminum (specific resistance 1.55×10^{-6} and 2.50×10^{-6} Ω cm for pure Cu and Al at room temperature, respectively) and could provide slightly better isolation, it is three times heavier than aluminum and much more difficult to machine. An aluminum alloy tube with a wall thickness of 20 mm was, therefore, used as the barrel. Internal dimensions of the hand made barrel are 140 mm (length) by 100 mm (diam-

eter) and provide ample room for placing compensation and modulation coils inside the sample compartment.

The linear sizes of the coils are in a range from 10 to 50 cm, and the attainable machining/assembling accuracy was estimated to be a conservative ±0.1 mm. Thermal "breathing" of the linear dimensions of the current elements result in changes on the same order of magnitude. The thermal expansion coefficients for Al and Cu are 23.3×10^{-6} and 16.7×10^{-6} K^{-1} at 300 K, respectively, and a 10 °C temperature rise would change the size of a 50 cm piece of aluminum by 0.1 mm. Thus, relative sizes of the current elements cannot be held better than about 10^{-4}, which sets the practical limit for attainable field accuracy. A 1 order of magnitude better field homogeneity (10^{-5}) was chosen as the target value for calculation of coils.

The sweeping system is divided into two subsystems, further referred to as the "scanning" and the "power" systems, which are optimized to perform slightly different tasks. The scanning system consists of two pairs of coils, is designed for maximum field homogeneity in the working region, and will scan the field from −100 to +100 G. In a yoke-free arrangement the power-to-field conversion efficiency drops as square of linear dimensions and field homogeneity improves as the coil sizes are increased. For this reason the coils are as large as practical, and the created field range was deliberately limited to ±100 G, which still allows performing complete experiments in the vicinity of zero field at a maximum power dissipation of about 250 W. The rate of field decay outside the working region was not considered, since the field there will never exceed a fraction of 100 G, which is acceptable.

The power system was optimized from a different perspective. The system is required to produce fields up to 400 G, and thus its efficiency becomes an important issue. Furthermore, due to a rather high field its profile not only in the working region but also outside it becomes critical. On the other hand, the system is required to work outside the 100 G range covered by the scanning system, where requirements to field homogeneity are less stringent. Thus a different compromise was reached. The power system is designed smaller than the scanning system and physically rests inside it and partly inside the barrel, which improves its efficiency at the price of certain loss of field homogeneity. The system is designed with active shielding, similar to approaches used in pulsed nuclear magnetic resonance (NMR),[10] and consists of three pairs of coils. One pair is wired in the opposite polarity, which significantly improves the rate of field decay outside the working region. The system will be operated from a unipolar power supply with electronically reversable +/− terminals, and the field is stepped in 50 G increments. The field of the opposite direction will be created by electronically reversing output terminals at the power supply unit. The home made system dissipates about 800 W at a nominal field of 400 G, so water cooling of the entire system is used.

The compensation system consists of two nearly identical pairs of rectangular coils placed inside the barrel along the Z axis, one pair for each of the X and Y directions. The nominal field of the pair is set to 1.5 G, and the geometry is optimized for maximum field homogeneity in the working region. Since the absolute values of the field are not large, efficiency and relative field homogeneity are not very critical for the compensation system.

III. CALCULATION

A. General approach

In calculating the parameters of the coils forming the sweeping system we first note that for a system of coaxial coils it is sufficient to optimize the field only on the axis, since field homogeneity on axis here automatically leads to field homogeneity in the adjacent cylindrical volume—the working region of the system. This allows using much simpler expressions for the field at the axis of a circular current, which are available in closed analytic form. After on-axis optimization is completed, we checked the resulting field homogeneity in the entire three dimensional (3D) region by numerical evaluation.

Next we choose the type of optimization. The first option is local optimization—trying to zero as many of the lower derivatives of the field at the point of optimization as possible. The best known example of this approach is Helmholtz coils—a pair of identical coaxial parallel circular coils that are exactly one coil radius apart from each other and are wired in the same polarity. Symmetrical coil positions force all odd derivatives to be zero at the midpoint between the coils—the center of the system. One free parameter that is available—the ratio of coil radius to intercoil distance—is then chosen so as to cancel the second derivative. Thus, the on-axis field of Helmholtz coils behaves as $B(\Delta z)=B_0+\alpha(\Delta z)^4$, where Δz is the small displacement from the midpoint along the axis. Addition of another pair of symmetrically placed identical coils with the same current brings about one more free parameter, which can be chosen so as to cancel the fourth derivative, and so on. This approach can yield very good field homogeneities, but only over a limited range of displacements from the point of optimization. However, we need field homogeneity in a rather long cylinder, so the other approach—global optimization—was adopted.

In global optimization the root-mean-square (rms) deviation of the field from the desired field profile over the entire region of optimization is minimized at the expense of certain field ripple across the region. More specifically, the following functional was minimized:

$$F=\int_{z_1}^{z_2}\left(\frac{B(z)-f(z)}{B(z_0)}\right)^2 dz, \tag{1}$$

where $[z_1,z_2]$ is the region of on-axis optimization, $f(z)$ is the desired field profile, $B(z)$ is the field created on axis by the system of current elements that is being optimized, and $B(z_0)$ is the field at the reference point–sample location and center of the system. We mostly followed the procedure suggested by Lugansky,[11] but varied not only the geometric parameters of the coils, but also their currents, so for each pair of coils three parameters were varied independently: radius, intercoil distance, and coil current. In calculations the integral was substituted with the sum over equidistant points

$$\delta = \sum_{i=1}^{M} \left(\frac{B(z_i) - f(z_i)}{B(z_0)} \right)^2. \quad (2)$$

The practical limit for the number of points M was found to be about 100, and its further increase did not improve results. Since the system is completely symmetric, optimization was carried out only over one half of the working region.

All optimizations were performed in a MATLAB[12] environment using the built-in routine *fmincon*. The on-axis field for a system of N circular currents with point cross section was calculated from the Biot–Savart law as

$$B(z) = \frac{\mu_0}{2} \sum_{k=1}^{N} I_k R_k^2 [R_k^2 + (z - Z_k)^2]^{-3/2}, \quad (3)$$

where $\mu_0 = 4\pi \cdot 10^{-7}$ N/m is magnetic permeability of vacuum, I_k, R_k, and Z_k are the current, radius, and half the intercoil distance (offset from the center) of the kth current element. The on-axis field for a system of N circular coils with finite cross sections was calculated as[9]

$$B(z) = \frac{\mu_0}{2} \sum_{k=1}^{N} J_k \left(\begin{array}{l} (z_{2k} - z) \ln \dfrac{a_{2k} + [a_{2k}^2 + (z_{2k} - z)^2]^{1/2}}{a_{1k} + [a_{1k}^2 + (z_{2k} - z)^2]^{1/2}} - \\ (z_{1k} - z) \ln \dfrac{a_{2k} + [a_{2k}^2 + (z_{1k} - z)^2]^{1/2}}{a_{1k} + [a_{1k}^2 + (z_{1k} - z)^2]^{1/2}} \end{array} \right), \quad (4)$$

where a_{1k} and a_{2k} are the inner and outer coil radii, z_{1k} and z_{2k} are the innermost and outermost coil Z coordinates, and J_k is the density of current in the kth coil. For convenience we introduce the positions of centers of the coil cross sections r_{0k} and z_{0k}, and their radial and axial thicknesses Δr_k and Δz_k, so that $a_{1,2k} = r_{0k} \mp \frac{1}{2} \Delta r_k$, $z_{1,2k} = z_{0k} \mp \frac{1}{2} \Delta z_k$.

The sequence of optimization of the sweeping system is as follows. First, the system of zero-cross-section ("thin") coils is optimized using Eq. (3). Then the cross sections of the coils are calculated from the obtained optimal values of coil currents I_k and preset coil current densities J_k. The different values of I_k are achieved by winding different numbers of turns of wire in the coil. All coils within each subsystem (scanning and power) will be wound from the same wire and connected in series, so the same current will be injected into each coil, and J_k values will be approximately equal across each subsystem.

The obtained cross sections are initially set to squares ($\Delta r_k = \Delta z_k$) and then optimized using Eq. (4), keeping their centers (r_{0k} and z_{0k}) fixed at the optimal position found for the thin coils. If optimization leads to overlapping of the "thick" coils in space, the process is repeated from the beginning with new seed values (search for r_{0k} and z_{0k}). After the cross section has been optimized, the winding is packed—the width and height of each cross section is adjusted so as to accommodate an integral number of turns of wire in each layer and an even number of layers, including the interlayer separators (*vide infra*). The current density J_k for imaginary homogeneous current flow across the cross section is then calculated for each coil taking into account the finite thickness of wire insulation and interlayer separators. For example, for the wire actually used with a diameter of copper of 1.4 mm and outer diameter $d = 1.5$ mm the fraction of the area wasted by insulation is $2\Delta d/d \approx 0.2/1.5 \approx 13\%$, i.e., rather substantial despite its thinness. Finally, r_{0k} and z_{0k} are fine tuned keeping Δr_k, Δz_k, and J_k fixed.

The procedure for optimization of the compensating system will be described later to avoid confusion, since it uses another choice of axes.

B. Power system with active shielding

First, the power system was synthesized with the following geometric restrictions: free internal cylindrical volume at least 10 cm (length) by 10 cm (diameter) for placing compensation system and sample holder assembly, the barrel wall thickness of at least 1 cm for passive ac shielding/structural strength and stability, the opening between innermost coils of at least 5 cm for manipulating the sample, and the length along the Z axis not more than 30 cm to place XRT not farther from the sample than needed. We sought for relative field homogeneity in the working region (±4 cm from center) not worse than 10^{-4}, and the field in the shielded region (farther than 15 cm away from center) not higher than $0.1 B_{\max}$. To account for the two regions of optimization, the penalty function Eq. (2) was taken as the sum of two contributions of the form

$$\delta = k \sum_{i=1}^{M} [B(z_i) - f(z_i)]^2, \quad (5)$$

where $f(z) \equiv 1$ and $k = k_1$ for $0 < z < l_1$ (inside the working region), and $f(z) \equiv 0$ and $k = k_2$ for $l_2 < z < l_3$ (in the shielded region). Since in the working region the homogeneity of the field is crucial, while in the shielded region only the smallness of the absolute value of the field is required, weight factors k_1 and k_2 were introduced, with setting $k_2 \ll k_1$ at the final iterations of the optimization procedure.

First, a system with two pairs of coils, the working one and the shielding one wired in the opposite polarity, was attempted, but the formulated requirements could not be satisfied with sensible values of parameters. For the best synthesized system relative field homogeneity in the working region was 4×10^{-3} with power dissipation in excess of 4 kW, which was considered unacceptable. Further simulations showed that a set of three pairs of coils, two working and one shielding, is a minimal configuration meeting the imposed requirements. Theoretically attainable relative field homogeneity in the working region for this configuration was found to be about 5×10^{-6} at a power consumption of about 800 W. The resulting field profile is shown in Fig. 2 with solid line, and features a rather abrupt decrease of field strength in the region of shielding (shown with arrows). An expanded view of field profile in the working region is shown with solid line in Fig. 3.

C. Scanning system

The scanning system was synthesized after the power system with additional geometric restrictions of being physically compatible with it. The field profile was optimized for maximum homogeneity inside the working region, without considering its exterior. Again, the simplest possible configu-

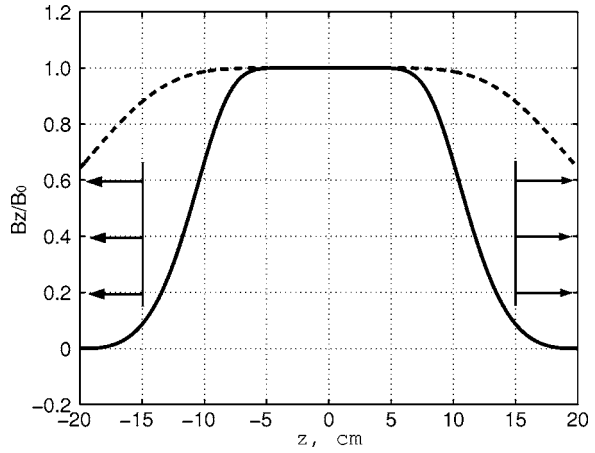

FIG. 2. Calculated normalized dependence of the axial component of magnetic field on the axis (Bz on axis) of the scanning system (without active shielding, dashed line, nominal field $B_0=100$ G), and the power system (with active shielding, solid line, nominal field $B_0=400$ G). Horizontal arrows mark the region of active shielding.

ration of one pair of coils would not yield the sought field homogeneities, and the configuration with two pairs of coils was chosen. The resulting field profile is given in Figs. 2 and 3 with dashed lines and should be compared with the profiles for the power system. The scanning system shows better theoretical field homogeneity in the working region (1.4×10^{-6} versus 4.3×10^{-6} for the power system) at the expense of a much shallower field profile decrease outside the region, with a rated power dissipation of about 200 W. The cross section of the entire sweeping system is shown to scale in Fig. 4.

The optimized parameters of the system, which were actually used for building the device, are summarized in Table I. Since the system is linear with respect to all dimensions, it can be scaled up or down as required by simultaneous linear scaling of all sizes. The actual calculations were in fact performed in reduced dimensionless variables, from which the physical dimensions of the coils were obtained by multiplying by dimensioning parameter L taken here to be 5

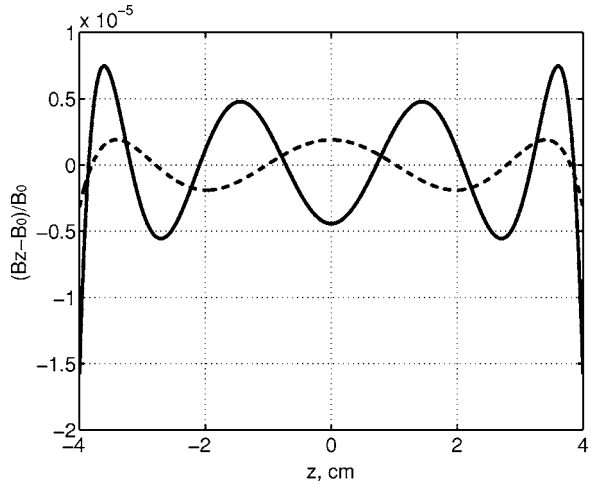

FIG. 3. Calculated relative deviation of Bz on axis of the magnetic systems within the working region (±4 cm from the center) showing the theoretically attained field homogeneity for the scanning (dashed line, nominal field $B_0=100$ G) and power (solid line, nominal field $B_0=400$ G) systems.

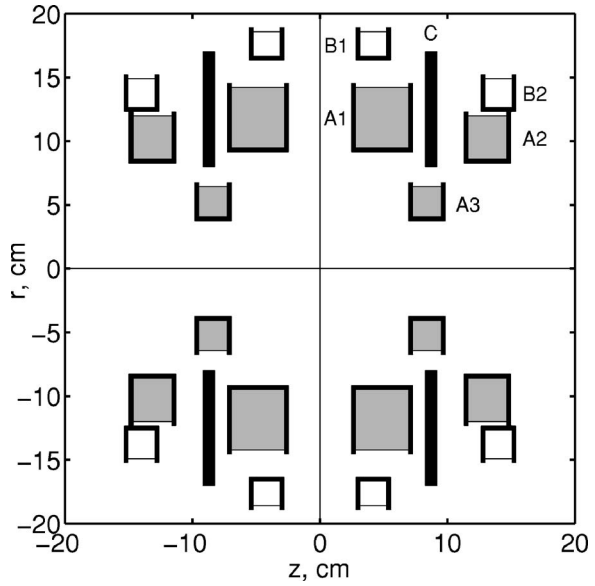

FIG. 4. Calculated cross sections and spatial arrangement of coils of power (A) and scanning (B) systems, and of the water-cooled disk of the cooling assemblies (C).

cm: $z=L\cdot z_{\mathrm{opt}}$, $r=L\cdot r_{\mathrm{opt}}$, $\Delta z=L\cdot\Delta z_{\mathrm{opt}}$, and $\Delta r=L\cdot\Delta r_{\mathrm{opt}}$. The actual current density in the coil, needed to create magnetic field $B(\mathrm{T})$, is given by $J(\mathrm{A\ m^{-2}})=\frac{5\times10^6}{\pi}\frac{B(\mathrm{T})}{L(\mathrm{m})}J_{\mathrm{opt}}$, total current in the coil $I(A)=\frac{5\times10^6}{\pi}B(\mathrm{T})L(\mathrm{m})I_{\mathrm{opt}}$.[9]

D. 3D field check

Hitherto all optimizations were performed on axis only, where simple closed expressions for the produced fields can be used. We now check the field in the entire working region using a numerical evaluation of expressions for radial $B_r(z,r)$ and axial $B_z(z,r)$ components of the field created by a circular current:[13]

$$B_r=\frac{\mu_0}{2\pi}I\frac{z}{r}[(r+a)^2+z^2]^{-1/2}\times\left(-K(k)+\frac{a^2+r^2+z^2}{(a-r)^2+z^2}E(k)\right),\tag{6a}$$

$$B_z=\frac{\mu_0}{2\pi}I[(r+a)^2+z^2]^{-1/2}\times\left(K(k)+\frac{a^2-r^2-z^2}{(a-r)^2+z^2}E(k)\right),\tag{6b}$$

where I is the current, a is its radius, $k^2=4ra/(r+a)^2+z^2$, and $K(k)$ and $E(k)$ are complete elliptic integrals of the first and second kind, respectively. In calculations the field from each N-turn coil was represented as the sum of fields from N equal circular currents with geometries corresponding to actual placement of each turn in the coil. The results of check calculations for the power system are shown in Figs. 5 and 6. As can be seen, the B_z field profile in the entire working region (±4 cm along the z axis and +0.5 cm along the r axis in cylindrical coordinates) is indeed practically identical to the on-axis field profile, and the radial field component is negligibly small. Similar results were also obtained for the scanning system.

TABLE I. Construction details for the sweeping system. All geometrical sizes are given with one decimal place (accuracy ±0.1 mm mm). All "total" characteristics refer to complete systems having two coils of each type and are given at room temperature. All coils of each system are wound with the same wire and are wired in series thus having the same nominal current.

	Power system			Scanning system		
	Coil A1	Coil A2	Coil A3	Coil B1		Coil B2
Axial center of cross section z_0 (mm)	48.6	131.4	83.7	41.6		140.0
Radial center of cross section r_0 (mm)	118.7	102.5	52.5	176.3		137.8
Axial thickness of cross section Δz (mm)	41.9	30.6	22.5	21.1		21.1
Radial thickness of cross section Δr (mm)	47.8	34.1	23.8	19.2		22.4
Inner axial border z_{min} (mm)	27.7	116.1	72.42	31.3		129.4
Outer axial border z_{max} (mm)	69.5	146.7	95.0	52.4		150.6
Inner radial border r_{min} (mm)	94.8	85.5	40.6	166.6		126.6
Outer radial border r_{max} (mm)	142.5	119.6	64.4	185.9		149.0
Wire gauge (diameter by copper, mm)	—	1.5	—	—	1.4	—
Turns in one layer	26	19	14	14		14
Number of layers	28	20	14	12		14
Turns in coil	728	380	196	168		196
Resistance (Ω)	5.3	2.4	0.6	2.1		1.9
Total resistance (Ω)	—	16.6		—	8	—
Nominal current (A)	—	7		—	5.8	—
Nominal voltage drop (V)		116			47	
Total measured inductance (mH),		89 @100 Hz			19 @100 Hz	
		60 @1 kHz			10 @1 kHz	
Maximum measured surface temperature rise (°C)			15			

E. Geometric stability check

After the geometry of the system was optimized, a check on the geometric stability of the system was performed to determine the degree to which minor deviations of geometric parameters from their optimal values can deteriorate field homogeneity in the working region. First, one of the parameters for the system of coils was slightly varied while keeping all other parameters at their optimal values, and the homogeneity of the on-axis B_z field was numerically evaluated. Figure 7 shows the results of this procedure for the power system as the dependencies of relative field homogeneity δB_z on relative deviation of coil radii or intercoil distances. The curves are fairly straight lines, as it should be for small deviations, and it can be seen that a deviation of 0.1 mm for the size of 10 cm (10^{-3}) spoils the homogeneity to several units times 10^{-4}, i.e., by 2 orders of magnitude as compared to the theoretical optimum.

This is a somewhat discouraging result. However, we note that there are several error-prone geometrical parameters in the system, not just one, and simultaneous deviations

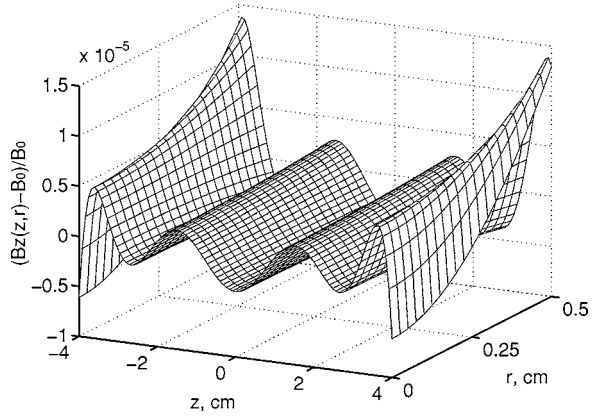

FIG. 5. 3D field check: calculated relative deviation of Bz in the cylindrical working region (8 cm long by 1 cm diameter) for the power system. Nominal field B_0=400 G.

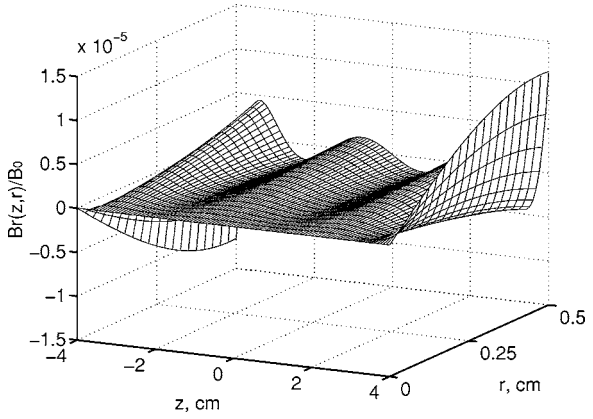

FIG. 6. 3D field check: calculated radial (Br) component of the magnetic field in the cylindrical working region (8 cm long by 1 cm diameter) for the power system relative to nominal field B_0=400 G.

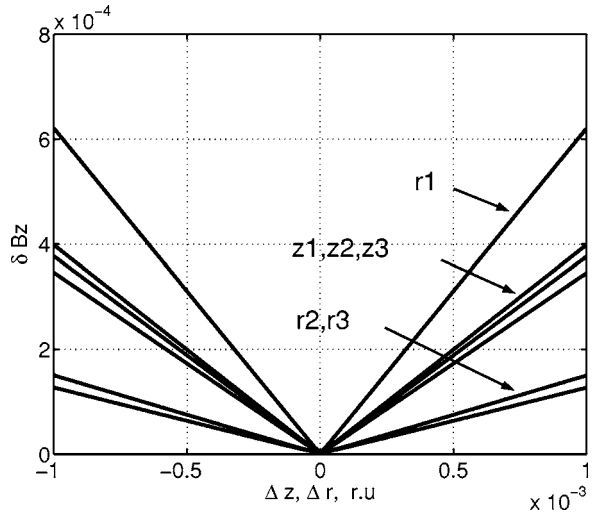

FIG. 7. Relative rms deviation of Bz component of on-axis field induced by symmetric deviation of one of the geometric parameters for one of the three pairs of coils for the power system. Other parameters are held constant and equal to their optimal values; $r1$–$r3$, $z1$–$z3$ are radii and offsets from the center, respectively, for the corresponding coil pair.

of several parameters from their optimal values could partly compensate each other. Figure 8 shows a histogram of relative homogeneity for an-axis B_z field of the power system in the working region for random distribution of relative geometric distortions in the range $\pm 10^{-3}$. To produce the histogram, the range of distortions was divided into five equal intervals, and the six parameters (three pairs of r_{0k} and z_{0k}) were erred covering all 5^6 possible combinations. For each configuration the homogeneity was then calculated and noted for plotting. As can be seen, the distribution has a well defined maximum at about 10^{-4}. Similar calculations were performed for the scanning system and gave similar results.

Thus we see that the absolute geometric inoptimality of parameters of 0.1 mm indeed limits the attainable relative field homogeneity at the level of 10^{-4}. The smallest coil is the most critical part as it shows larger relative deviations. Further improvements are possible only by fine tuning currents in the coils. The geometry of the coils can be (and has been) optimized to much better field homogeneity, down to 10^{-6} and better, but the system becomes progressively more and more sensitive to minor deviations of parameters. Choosing a realistic target homogeneity of 10^{-4} produces much shallower minima with respect to optimization parameters and thus provides for a much more stable experimental device.

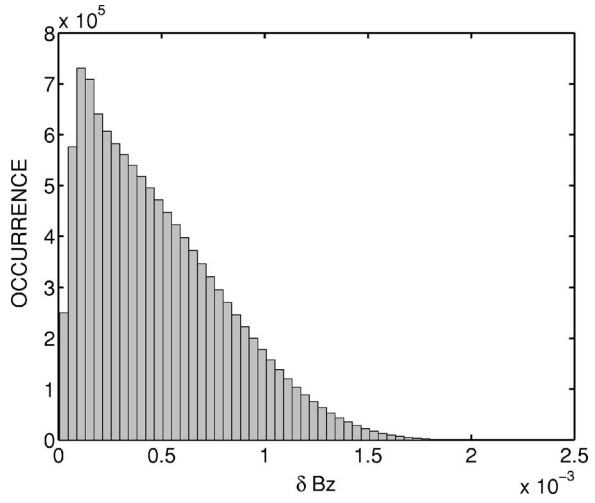

FIG. 8. Distribution function of the homogeneity parameter (rms deviation of Bz component of magnetic field) for the power system.

F. Compensation system

After the sweeping system was optimized and the geometry of the barrel was defined, the compensation system was designed to physically fit inside the barrel. The compensation system consists of two pairs of thin rectangular coils, one pair for each of two mutually perpendicular Cartesian axes in the plane normal to the axis of the sweeping system and passing through the origin of the system. Each coil is modeled as four straight current-carrying bars assembled into a planar rectangular shape. To calculate the field of a single rectangular coil we choose the following Cartesian coordinate system: origin at the center of the coil, W axis normal to the plane of the coil, and U and V axes parallel to the sides of the coil. The field (B_u, B_v, B_w) at an arbitrary point (u, v, w) is then given by the following expressions:[14]

$$B_u(u,v,w) = \frac{\mu_0 I}{4\pi} \sum_{i=1}^{4} (-1)^{i+1} \frac{w}{r_i(r_i + v_i)}, \tag{7a}$$

$$B_v(u,v,w) = \frac{\mu_0 I}{4\pi} \sum_{i=1}^{4} (-1)^{i+1} \frac{w}{r_i(r_i + u_i)}, \tag{7b}$$

$$B_w(u,v,w) = \frac{\mu_0 I}{4\pi} \sum_{i=1}^{4} (-1)^{i} \frac{v_i(u_i + v_i) + u_i^2 + v_i^2}{r_i(r_i + u_i)(r_i + v_i)}, \tag{7c}$$

where $u_1 = u_4 = u + a$, $u_2 = u_3 = u - a$, $v_1 = v_2 = v + b$, $v_3 = v_4 = v - b$, a and b are half the lengths of the sides of the rectangular coil, and r_i is the distance from the ith corner of the coil to the point of observation.

The goal of optimization was to find geometric parameters of two symmetrically placed identical parallel coils that would provide maximum global relative homogeneity of the B_w field of the pair (normal to the axis of main field sweeping) in a cylinder 8 cm long by 1 cm in diameter (working region) along the U direction of the pair (the axis of sweeping). It is clear that the longer the coils are the better the homogeneity can be inside the rather long working region. The coils were made, therefore, as long as allowed by the internal dimensions of the barrel. The width of the coils was also limited to the maximum allowed by the internal radius of the barrel. This left just one parameter for optimization—the distance between the coils of each pair, while requiring both pairs to inscribe into the barrel, to be spatially compatible with each other, and to have equal intercoil distances to maximize the internal volume. The optimal intercoil distance was found to be 0.95 of the barrel internal radius. Table II lists the parameters of the optimized coils, and Fig. 9 shows the calculated field profile.

TABLE II. Construction details for the compensation system. All geometrical sizes are given with one decimal place (accuracy ±0.1 mm). All "total" characteristics refer to complete systems of two coils. Both coils of each system are wound with the same wire and are wired in series thus having the same nominal current. All sizes refer to the centers of 3×3 mm copper cross sections.

	X coil	*Y* coil
"2*a*" length of the longer side of coil (mm)	129.8	115.8
"2*b*" length of the shorter side of coil (mm)	112	112
Intercoil distance for the pair (mm)	62.1	62.1
Cross section of winding (mm×mm)	3×3	3×3
Wire gauge (diameter by copper, mm)	0.3	0.3
Turns in coil	80	80
Resistance (Ω)	10.2	9.3
Total resistance (Ω)	20.4	18.6
Nominal current (A)	0.25	0.25
Nominal voltage drop (V)	5.1	4.7

IV. BUILDING AND TESTING

A. Building particulars

The synthesized system was built according to the found specifications. Construction details for the sweeping system are collected in Table I.

Figures 10–12 show the cross section of the sweeping system resting on and partly inside the barrel, a schematic view of the compensation system insert that goes inside the barrel, and a photo of the working system, respectively. Referring to Fig. 10, symbols A_i and B_j mark the cross sections of the coils of the power and the scanning systems, respectively. Also shown are the two identical cooling assemblies (identified as *C*) each consisting of a 3 mm thick copper disk with a 6 mm water-carrying brass tube soldered to its outer perimeter, which is pressed between two solid aluminum alloy disks that in turn are in thermal contact with the coils. Each cooling assembly is held together with twelve 8 mm threaded brass studs with brass nuts and washers (seen in Fig. 12). The gaps between the copper disk and the aluminum sides are filled with thermogrease. The two assemblies

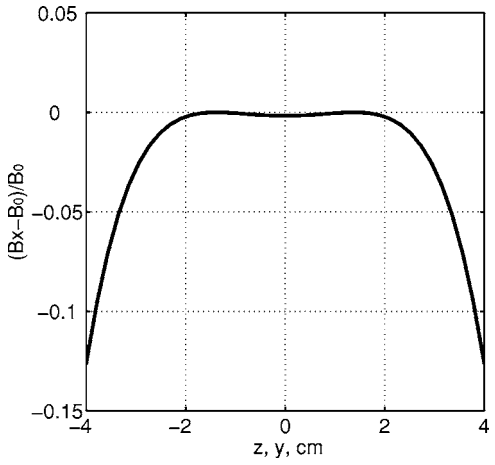

FIG. 9. Calculated relative deviation of *Bx* (normal to the plane of the rectangular coils) component of magnetic field from one pair of compensation coils as a function of *z* (along the axis of the spectrometer parallel to the plane of the rectangular coils). Nominal field B_0=1.5 G.

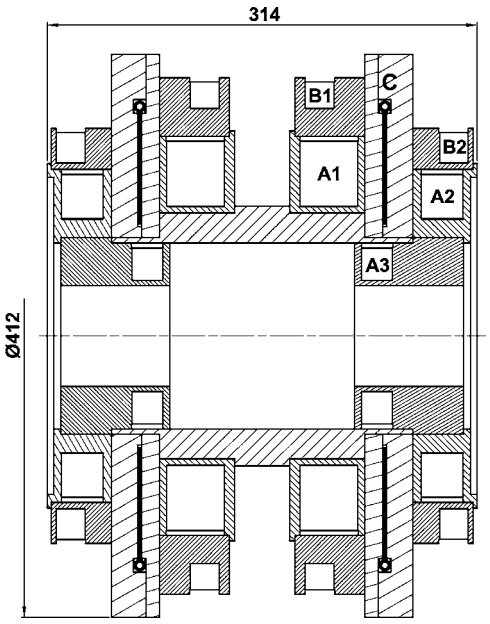

FIG. 10. Cross section of the actually built magnetic system: (A) power, (B) scanning magnetic systems, (C) cooling assembly. Compensation system not shown for clarity.

C are connected in series and fed with tap water. They also serve as important construction elements, as can be seen in Fig. 12.

All coil bobbins are made from aluminum alloy, and all aluminum–aluminum contacts are lubricated with graphite grease to prevent seizing. The entire system is held together as a packet with eight long threaded brass studs (not shown) going through the entire sweeping assembly from end to end passing through channels drilled in the walls of the barrel.

The parameters of the sweeping coil winding are given in Table I. Copper sheet interlayer separators, 0.1 mm thick, were put between the layers of the winding to improve the regularity of the winding pattern. Although putting the turns

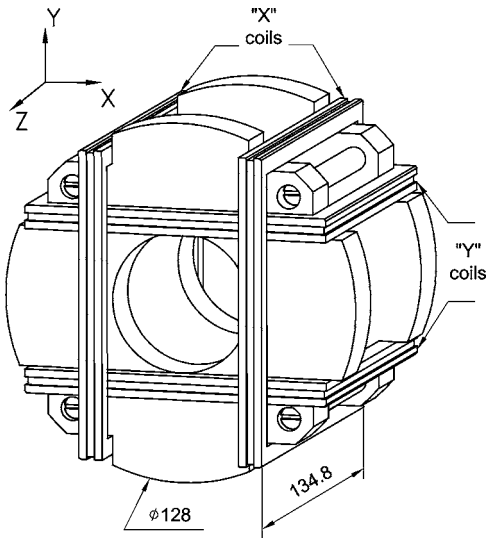

FIG. 11. Compensation system assembly. The global axes of the sweeping system are given for reference. Coil pair *X* compensates the *x* component, and coil pair *Y* the *y* component of the residual magnetic field of the laboratory.

FIG. 12. Photo of the actually built magnetic system, including a 30 cm scale bar.

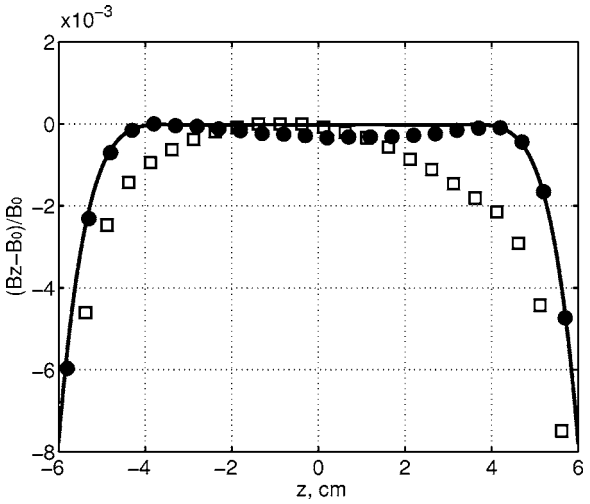

FIG. 13. Relative deviation of Bz on axis for the power system: theoretical calculation (solid line), measurements for optimal (calculated) geometrical parameters (filled circles), and measured Bz field component with z offsets for all coils uniformly reduced by 0.5 mm from their optimal values (open squares). Reference measurement field B_0=450 G.

of the next layer in the pits of the underlying layer would have yielded higher packing efficiency, it was found that in practice the regular pattern does not persist for more than several layers from the flat bottom of the coil. To this end a thin but rigid enough copper sheet was used as the flat bottom for each layer. To secure the windings and improve their heat conductance, each layer was coated with alumina-filled epoxy resin after winding, and the complete coil was left to cure at room temperature. Experimentally it was found that prolonged operation of the sweeping system at rated power (up to 1 kW) leads to a temperature rise of not more than 15 °C for ambient temperature 20 °C and tap (cooling) water temperature 15 °C. The thermal "breathing" of the system was therefore sensibly low and within the prescribed tolerances.

The parameters of the compensation coil windings are given in Table II. All elements of the compensation system insert (Fig. 11) are machined from fiberglass/epoxy composite. One of the coil pairs (Y coils in Fig. 11) is made slightly shorter and rests inside the other pair (X coils). The system is mechanically rigid enough and can be easily inserted inside the barrel. It also leaves enough free volume inside for placing the sample holder, and gives free access along all the six semiaxes to the sample location. As can be seen in Fig. 12, the barrel has four access ports in the XY plane. The completed system was immediately dubbed "bathyscaphe" after assembling because of its resemblance to the deep-water vehicle.

B. Magnetic field measurements

Since the designed systems are linear with respect to the injected currents, the magnetic field measurements accented the determination of the relative profiles and relative homogeneities at or near the highest attainable fields giving results valid near zero field. The only absolute measurements taken were of the current to field conversion ratios (CFCRs). The CFCR for the power system was measured and calibrated using a NMR gaussmeter SH1-9 at the maximum field we could create (450 G), and was found to be equal to the expected value (57.18 G/A) within the measurement precision. Since the maximum field of the scanning system (100–120 G) could not be measured with the available NMR meter, the CFCR for the scanning system (17.2 G/A) was calibrated using a Hall probe gaussmeter and the power system as reference.

All relative magnetic field measurements were performed with a modified Hall probe gaussmeter SH1-8. The meter itself has an analog indicator, the signal from which was tapped and passively filtered (time constant was raised to 15 s). The filtered signal was then read with a digital microvoltmeter used as a zero indicator. The accuracy of measurements was limited by the absolute field magnitude at which the profile was being taken, and by the long-time drift of the (analog) gaussmeter. Experimentally it was found that for the 450 G field created by the power system with its 8 A power supply and a measurement time of 1 h or shorter the results were reproducible to within 10^{-4}—the target accuracy of this work. For the scanning system the measurements were taken at 120 G, created by feeding 7 A from the power supply of the power system into the 100 G nominal field system. The accuracy of measurement was correspondingly about four times lower, or about 4×10^{-4}. For the compensation system the measurements were performed at 15 G, ten times the rated field of the system, about as much as the coils would withstand without fatally overheating. The relative error of these measurements is estimated as 10^{-2}.

The carrying barrel of the system was designed to allow a 0.5 mm margin for physical displacement of the coils along the Z axis using thin copper shims to fine tune the locations of the coils. Figure 13 shows the calculated on-axis field B_z profile for optimal geometry of the power system (solid line), the measured field profile for optimal geometry of the system

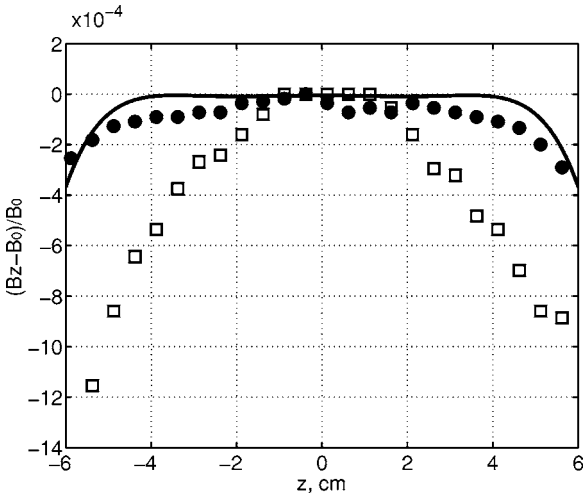

FIG. 14. Relative deviation of Bz on axis for the scanning system: theoretical calculation (solid line), measurements for optimal (calculated), geometrical parameters (filled circles), and measured Bz field component with z offsets for all coils uniformly reduced by 0.5 mm from their optimal values (open squares). Reference measurement field $B_0=120$ G.

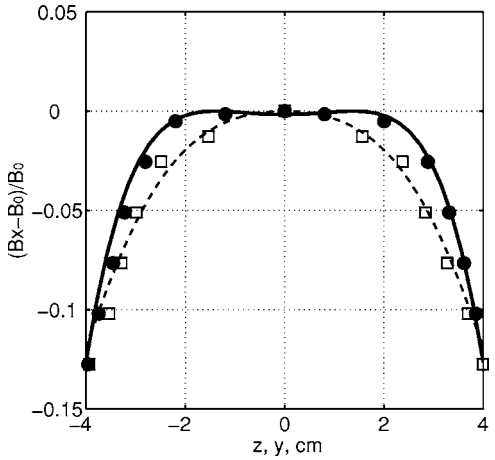

FIG. 16. Relative deviation of Bx (normal to coil plane and spectrometer axis, see Fig. 11) component of magnetic field from coil pair X of the compensation system along the z axis: theoretical calculation (solid line) and measured values (filled circles), and along the y axis: theoretical calculation (dashed line) and measured values (open squares). Reference measurement field $B_0=15$ G.

(filled circles), and the measured field profile with z displacements of all coils from the center uniformly reduced by 0.5 mm (open squares). The relative rms deviations of the measured B_z values on the axis of the working region were found to be about 1.5×10^{-4} (comparable to the measurement accuracy) for the optimal geometry, and about 2×10^{-3} for the distorted configuration.

The effect of geometric distortion can be alleviated by fine tuning currents in the coils of the system. Thus, shunting both coils A1 of the power system with rather large and slightly different resistors (209 and 189 Ω, for coils A1 with nominal resistance 5.3 Ω) completely removed the observed asymmetry of the field profile and restored the field homogeneity back to the target figure of 10^{-4}. However, this seemingly simple and efficient method has a drawback. The winding of the coil grows warmer during operation, and the measured 15 °C temperature rise leads to a 6% increase of coil resistance. Since the shunt bleeds about 2.6% of the current from the coil it is correcting, this in turn produces about 1.5×10^{-3} change of the current through the coils and a twofold drop of field homogeneity. Thus, this method of fine tuning can either be used for ultimate refinement of an already good field profile, or some sort of temperature stabilization, or control of current sharing between the coil and its shunt is needed, which would significantly complicate the system.

A set of similar graphs for the scanning system is shown in Fig. 14. Here again, the measured field homogeneity in the working region for the optimal geometry is about 10^{-4} and does not exceed the measurement uncertainty. Figure 15 shows the calculated and measured B_z field profile for the power system as a function of radial position. Figure 16 shows the calculated and the measured B_x field profiles from one pair of coils of the compensation system.

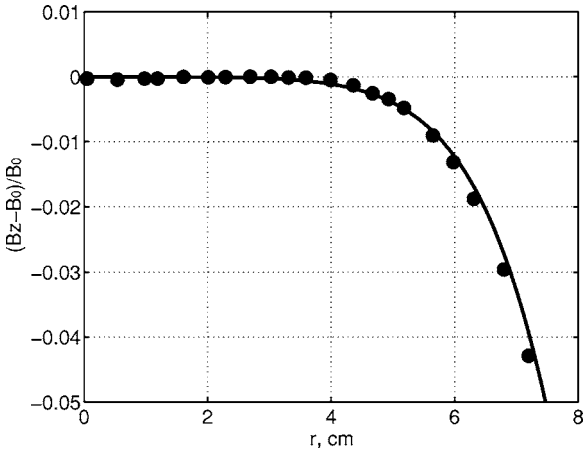

FIG. 15. Relative deviation of the axial (Bz) for the power system as a function of radial position from the center, in the plane normal to the axis, and passing through the center: theoretical calculation (solid line) and measurements for optimal (calculated) geometrical parameters (filled circles). Reference measurement field $B_0=450$ G.

ACKNOWLEDGMENTS

The authors are indebted to Professor Yuri Molin for valuable input in the course of this work and Dr. Fyodor Sviridenko for his help in preparing the manuscript. Comments from their colleagues in the laboratory were also very helpful. The switched mode power supply for the system was designed and built by Lev Medvedev. The work was supported by RFBR, Project No. 03-03-32331, and MinVuz, Project No. E02-5.0-49. D.V.S. is grateful to the Russian Science Support Foundation for awarding a personal scholarship.

[1] Portions of this work presented at the Conference "Magnetic Measurements 2004" held in Prague, Chezk Republic in July, 2004 and published in the Proceedings of the Conference in J. Electr. Eng.55, 77 (2004).
[2] K. M. Salikhov, Yu. N. Molin, R. Z. Sagdeev, and A. L. Buchachenko, *Spin Polarisation and Magnetic Effects in Radical Reactions* (Elsevier, Amsterdam, 1984).
[3] *Dynamic Spin Chemistry*, edited by S. Nagakura, H. Hayashi, and T. Azumi (Kodansha, Ltd. and Wiley, New York, 1998).

[4] Charles P. Poole, *Electron Spin Resonance: A Comprehensive Treatise on Experimental Techniques* (Dover, New York, 1997).
[5] *The Hanle Effect and Level Crossing Spectroscopy*, edited by G. Moruzzi and F. Strumia (Plenum, New York, 1991).
[6] F. B. Sviridenko, D. V. Stass, and Yu. N. Molin, Mol. Phys. **101**, 1839 (2003).
[7] D. V. Stass, B. M. Tadjikov, and Yu. N. Molin, Chem. Phys. **235**, 511 (1995).
[8] D. V. Stass, N. N. Lukzen, B. M. Tadjikov, and Yu. N. Molin, Chem. Phys. Lett. **233**, 444 (1995).
[9] C. R. Timmel, U. Till, B. Brocklehurst, K. A. McLauchlan, and P. J. Hore, Mol. Phys. **95**, 71 (1998).
[10] P. Mansfield and B. Chapman, J. Phys. E **19**, 540 (1986).
[11] L. B. Lugansky, J. Phys. E **20**, 277 (1987).
[12] © The MathWorks, Inc., website ⟨http://www.mathworks.com⟩.
[13] D. Bruce Montgomery, *Solenoid Magnet Design: The Magnetic and Mechanical Aspects of Resistive and Superconducting Systems* (Wiley-Interscience, New York, 1969), Chap. 8.
[14] J. Malmivuo, J. Lekkala, P. Kontro, L. Suomaa, and H. Vihinen, J. Phys. E **20**, 151 (1987).